Available online at www.sciencedirect.com

ScienceDirect

Energy Procedia 85 (2016) 329 – 338

Energy Procedia

Sustainable Solutions for Energy and Environment, EENVIRO - YRC 2015, 18-20 November 2015, Bucharest, Romania

Accurate measurements and analysis of the thermal structure of turbulent methane/air premixed flame

Constantin Levenţiu[a*], Bruno Renou[b], Sterian Dănăilă[a], Dragoş Isvoranu[a]

[a]*Faculty of Aerospace Engineering, University Politehnica of Bucharest, Splaiul Independentei 313, RO-060042, Bucharest, Romania*

[b]*CORIA - UMR6614, Université et INSA de Rouen, Campus du Madrillet - BP 8, 76801 Saint Etienne duRouvray Cedex, France*

Abstract

This paper provides further experimental and numerical results concerning the premix turbulent combustion of lean methane-air mixture. For V-shaped flame, the experimental data were acquired by two-dimensional Rayleigh scattering technique. The main purpose of this investigation is to obtain quantitative information on the instantaneous thermal structure of the flame front for both laminar and turbulent conditions. Four values for turbulence intensity have been considered. The flame surface density is closely related to the two-dimensional temperature gradient. For turbulent combustion, a general decreasing trend of averaged temperature gradient was observed. However, this tendency is inverted for very high turbulence intensity when the instantaneous temperature gradient presents high fluctuations. The flame front thickness PDF and the curvature PDF decrease with the turbulence intensity. The joint PDF of curvature and the maximum of the progress variable's gradient have the tendency to rotate counterclockwise with the increase of turbulence intensity. Negative curvature brings more energy in preheat zone of flame and enhances combustion; consequently the temperature gradients increase.

Peer-review under responsibility of the organizing committee EENVIRO 2015

Keywords: Laminar turbulent combustion; flame front structure

* Corresponding author. Tel.: +40723566065; fax: +40213181007.

E-mail address: cleventiu@yahoo.com.

Peer-review under responsibility of the organizing committee EENVIRO 2015

doi:10.1016/j.egypro.2015.12.259

1. Introduction

In spite of their significant role in environmental contamination, fossil fuels still represent, due to their high availability and volumetric energy density, the primary source of global energy production. Lean premixed combustion is one of the most promising concepts for substantial reduction of pollutant emissions because it reduces the burning temperature, therefore leading to a reduction of NOx emission. Development of efficient combustion devices in a rapid and cost-effective manner requires predictive models that should be, as much as possible, universal and robust. Modeling a premixed flame in a turbulent flow environment remains a challenging task due to the non-linear coupling between the time and length scales of turbulence structures and those of the combustion process. Usually, the different turbulence-combustion interaction types are indentified by so-called combustion diagrams [1]. The turbulent combustion model can be identified given the turbulence intensity, the laminar burning velocity, the turbulence integral scale, the laminar flame thickness and the value of the Karlovitz number. From this point of view, the following regimes are usually encountered: flamelets regime and pocket or distributed reaction zones, respectively.

Usually, the turbulent burning rate is estimated in respect to flame surface density. However, the flame surface density is directly related to the temperature gradient. Consequently, to validate or to develop new turbulent combustion models, the accurate measurements of temperature gradients and of the flame structure have to be provided.

The flame surface density may be determined by using statistical processing of experimental measurements of temperature and its gradient [2] or by geometric methods [3]. For Bunsen flames, surface density distributions were reported by Deschamps et al. [4], Lee et al. [5], Chen and Bilger [6] and Bell et al. [7] and for V-flames by Shepherd [3] and Veynante et al. [8,9]. Flat flames were considered by Shepherd and Cheng [10], Shepherd et al. [11]. Lawn and Schefer [12] addressed the low-swirl and diffuser type burners, Renou et al., [13] the freely propagating flame, while Shy et al. [14] the cruciform burner. The profiles of surface density reported by Veynante et al. [9] are tall and narrow at upstream locations. The profiles become shorter and wider at downstream locations because the brush thickness increases due to turbulent diffusion. A similar trend is observed by Bell et al. [7] for the Bunsen burner. More recently, Sweeney et al. [15] presented a comparison of different method that can be used to calculate the surface density.

The paper is organized as follows. First, the experimental arrangement and the operating condition are described. Second, Rayleigh scattering theory and post-processing method are briefly introduced. In the last part, validation of the measurement for laminar flame with numerical results and turbulence influence on the flame front structure are presented.

2. Experimental setup

The experimental setup consists of a vertical wind tunnel (Fig. 1) adapted for laminar and turbulent combustion. Fuel and air are mixed far upstream from the burner nozzle to obtain a perfectly homogeneous mixture. Both fuel and air are filtered by high-efficiency filters (filtering efficiency is more than 99.9% for 0.1 mm particles) to avoid Mie scattering for small particles.

The flow is laminarized with a divergent-convergent channel and a series of screens and honeycombs providing a very low velocity fluctuation of u'=0.06 m/s for an average velocity of 4 m/s. At the exit of the convergent, a V-shaped flame is anchored on a 1 mm diameter heated rod. The rod is mounted on the central axis of the square exit section (80mm x 80mm). To avoid the effect of lateral mixing layers, the analysis zone (18×6.5 mm) is chosen in the near-field, located at 35 mm above the heated rod.

To obtain Rayleigh scattered images, this area is illuminated with a Nd-YAG laser (10Hz, 630mJ/pulse) with a second harmonic generating crystal that produced a Q-switch output in □=532 nm. Experimental scheme is shown in Fig. 2. The laser sheet is obtained by a combination of one spherical and two cylindrical lenses. Scattered light is filtered by Melles Griot CG-KG-3-2x2-2 and Croma ZET 532/10 filters to suppress flame chemiluminescence and to isolate the frequency of 532nm. Images are captured with a Photometrics CoolSNAPHQ2 696×520 resolution CCD camera, characterized by 2x2 binning and 12bit digitizer. A magnification ratio of 38.2 pixel/mm is obtained with a Micro-Nikkor 105 mm f/2.8 lens.

To ensure correct measurements, the spatial resolution of the optic system is determined using the Modular Transfer Function (MTF) which is Fourier transform of the Line-Spread Function (LSF). To avoid aliasing problems [16], the LSF (Fig.3) is computed with respect to measured Step Response Function (SFR).

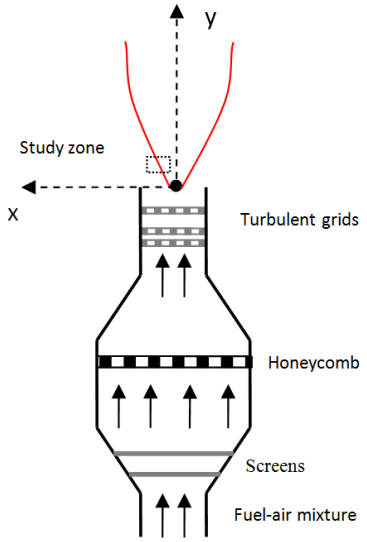

Fig. 1: Experimental setup

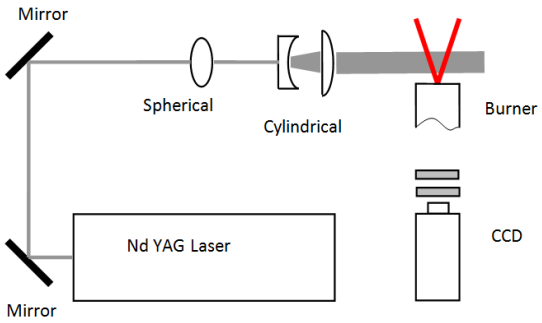

Fig. 2: Optical setup of 2D Rayleigh imaging technique

The spatial resolution of the camera is considered as the limit of the two consecutive black lines which cannot be distinguish (the contrast is less than 10%). It is twice of the inverse cutoff frequency of the MTF (Fig.4). The CCD camera Photometrics CoolSNAPHQ2 with a Micro-Nikkor 105 mm f/2.8 lens has spatial resolution of 0.268 mm, assuring accurate measurements of the flames with thickness of about 1 mm.

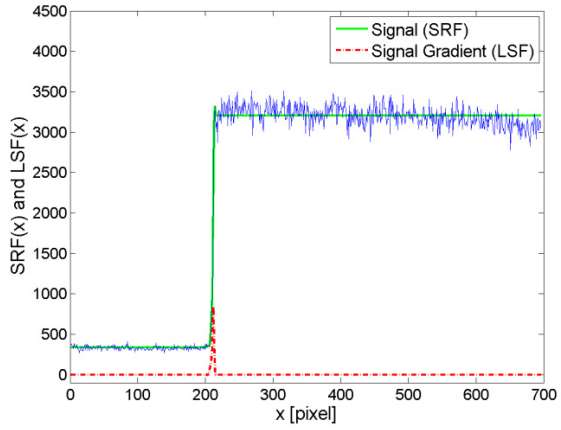

Fig. 3: Line-spread function (LSF) and step response function (SRF) for CoolSNAPHQ2 camera

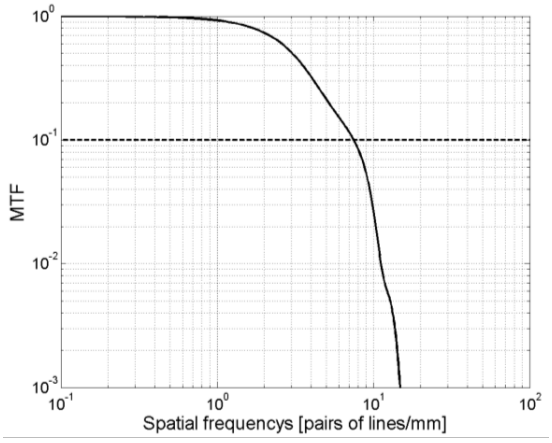

Fig.4: Modulation transfer function (MTF) for CoolSNAPHQ2 camera

An isotropic and homogeneous turbulent flow is generated by using perforated plates located upstream the rod. Different blockage ratios and net sizes are used to vary by an order of magnitude the level of turbulence. For the highest turbulence regime MH, a new type of turbulence generator called “Multi-Scale Turbulence Injector” (MoSTI) [17] has been designed and tested in the CORIA laboratory. The MoSTI injector is made of three

perforated plates shifted in space such that the diameter of their holes and blockage ratio increase with the downstream distance. MoSTI injector provides higher turbulence kinetic energy distributed over a large range of scales. Moreover, this injector allows to obtain an isotropic and homogenous high intensity turbulent flow at moderate Reynolds number values ($Re_\lambda \approx 80$, where λ is the Taylor microscale)

Four lean turbulent premixed methane-air flames at equivalence ratio of ϕ=0.6 were investigated. The laminar flame speed and laminar flame thickness are S_L=0.11 m/s and δ_L=1.02 mm, respectively. The regimes are summarized in Table 1, where Λ_u is integral length-scale, Ka is Karlovitz number (ratio of the chemical time scale to the Kolmogorov turbulent time scale) and Da is Damköhler number (ratio of the integral turbulent time scale to the chemical time scale).

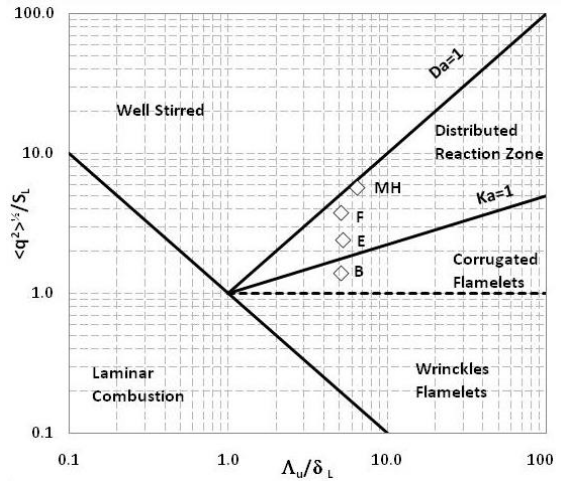

Fig. 5: Location of the investigated y regimes in the combustion diagram

Table 1. Investigated turbulent flames

Regime	u' [m/s]	Λ_u [mm]	Ka	Da
B	0.15	5.18	0.7	3.6
E	0.26	5.35	1.6	2.1
F	0.41	5.21	3.2	1.3
MH	0.63	6.6	7.6	0.9

Locations of investigated regimes in the combustion diagram follow a quasi constant integral turbulent length scale (Fig. 5), starting from a relatively low turbulence intensity (corresponding to corrugated flamelets domain) and reaching a very high turbulence (in the thin reaction zone).

3. Rayleigh scattering

The basic principle of Rayleigh scattering measurement is the elastic interaction between an incident laser light and a gas molecule. For a gas with various components, the local Rayleigh scattering signal is given by:

$$S_R(x,y) = I_0(x,y,\lambda)\, C\, N_d(x,y) \sum_i \chi_i(x,y)\sigma_i, \tag{1}$$

where $I_0(x,y,\lambda)$ is the incident laser light intensity, N_d is the total molecular number density, χ_i is the mole fraction of each different species or molecules and σ_i represents the Rayleigh scattering cross-section for each species. The calibration constant C takes into account the optical collection efficiency and characteristic lengths of the laser sheet imaged on the detector. Under constant-pressure condition and the ideal gas law assumption, the temperature field can be directly obtained from the Rayleigh signal S_R:

$$T(x,y) = T_0(x,y)\sigma_N S_R^0(x,y) / S_R(x,y), \tag{2}$$

where S_R^0 is the reference scattering signal taken at a reference temperature $T_0(x,y)$ with normalized cross section σ_N:

$$\sigma_N(x,y) = \sum_j \chi_j(x,y)\sigma_j \Big/ \sum_i \chi_i(x,y)\sigma_i . \tag{3}$$

Indices i and j denotes the i and j species present in the fresh/burnt gases, respectively. The normalized cross section σ_N is calculated from species mole fractions obtained with CANTERA code using a GRI3.0 mechanism. The refractive indices are calculated either by polynomial formulation [18] or by summation of atomic contribution.

Due to uncertainty of normalized cross section evaluation, four methods available in the literature are tested. The simplest one assumes a constant unitary value for the normalized cross section (Met. I). The second method (Met II), requires two data sets: one experimental and one numerical (see Lafay et al. [19] for details). The third method (Met. III) estimates the temperature by an empirical formula [20]:

$$c_T(x,y) = \frac{T(x,y) - T_u}{T_{ad} - T_u} = C_a \left[\frac{S_R^0(x,y)}{S_R(x,y)} \right] - C_b , \tag{4}$$

where the progress variable $c_T(x,y)$ is related to the measured Rayleigh scattering signals. The constants C_a and C_b depend on the equivalence ratio and are derived by curve-fitting from simulation of laminar flame. For equivalence ratio of 0.6 the constants are C_a=0.2066 and C_b=0.2036.

A similar formula (Met. IV) is proposed by Chen and Bilger [21]:

$$c_T(x,y) = C_a \left[\frac{S_R(x,y)}{S_R^0(x,y)} - C_b \right]^{-C_c} - C_d . \tag{5}$$

The fitting constants (C_a= 0.4411, C_b= 0.0956, C_c= 0.4800, and C_d= 0.4647) at equivalence ratio of 0.6 are obtained from numerical prediction of laminar flame.

4. Results

4.1. Laminar flame

To validate the experimental setup, the experimental data and the numerical prediction of CANTERA code are compared. The profiles of the temperature gradient against progress variable c are plotted in Fig. 6. Progress variable is a dimensionless temperature which is zero for reactants and one for burn products and is defined as:

$$c = \frac{T - T_u}{T_b - T_u} \tag{6}$$

where T_u is the fresh gas temperature and T_b the burnt gas temperature. For experimental data, the results obtained with all four methods previously presented are represented. In Table 2, $\nabla c_{\max}$ represents the maximum value of the gradient of the progress variable and the symbol Err refers to the relative error with respect to numerical results. Since the variation of the progress variable gradient along the flame front is less than 5%, all methods are in good agreements with the numerical results, especially in the reactant side of the flame. Method II provides best approximation for the temperature of burned gas; however the position and the value of the maximum progress variable are less accurate predicted. Method III was adopted herein because it provides the best global accurate correspondence with numerical results. it.

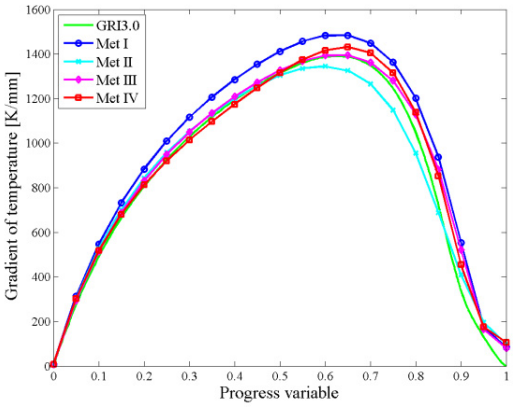

Fig.6. Gradient of temperature calculated with different methods for normalized cross section.

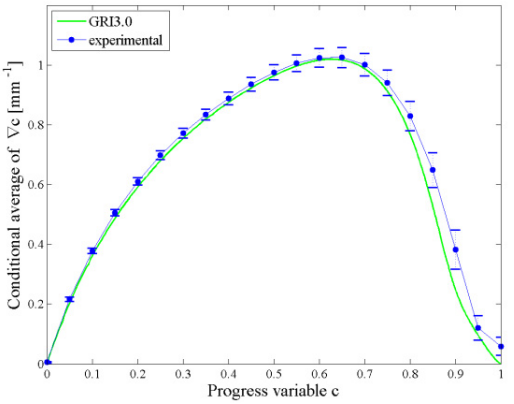

Fig.7 The progress variable gradient and its STD in laminar regime.

Table 2. Results for the temperature statistics for the different methods.

Method	T_b [K]	Err T_b [%]	∇c_{max}	Err ∇c_{max} [%]	$c_{\nabla c\ max}$	Err $c_{\nabla c\ max}$ [%]
GRI3.0	1665	-	1.019	-	0.628	-
Method I	1708	2.55	1.088	6.77	0.628	0.05
Method II	1667	0.09	0.986	3.24	0.595	5.25
Method III	1627	2.30	1.025	0.59	0.628	0.03
Method IV	1688	1.36	1.047	2.75	0.647	3.03

To assess the effect of the measurement uncertainties,the standard deviation of the gradient of the progress variable was plotted in Fig. 7. Small values of the standard deviation, as obtained, avoid the presence of false peaks in turbulent conditions.

4.2. Turbulent flame

For turbulent combustion, the flame front is no longer smooth; turbulence broadens it and can chang its structure. For low turbulent intensity (Fig. 8), flame front undulates but keeps the laminar flame structure. Instead, for high turbulent intensity (Fig. 9), turbulent structures begin to interact with the combustion process can break the flame front causing the appearance of islands in which combustion occurs. Also, the flame front thickness begins to vary having higher or lower values compared to laminar value.

Results of the progress variable gradient and uncertainties for turbulent flame regime B, E, F and MH at equivalence ratio of 0.6 are presented in Fig. 10. As expected, for turbulent flames, we obtain lower values then the laminar flame profile (green line), since we capture only two components of gradient. The general trend shows a decrease of gradients with turbulence intensity. However, a weak increase of gradients for highest turbulent intensity case MH was observed. The same order of magnitude of the integral-time scale and chemical time-scale (Damköhler number close to unity) seems to have a strong impact over the local flame structure. Also, the standard deviation increases since, with turbulence intensity, the flame front becomes more and more wrinkled and not aligned with the measurement plane.

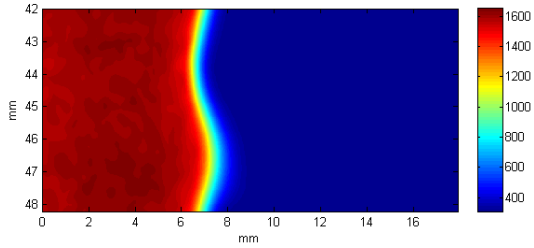

Fig.8. Temperature distribution for turbulent regime B

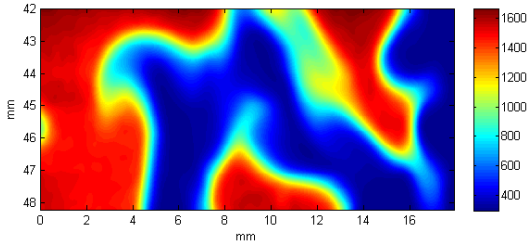

Fig.9. Temperature distribution for turbulent regime MH

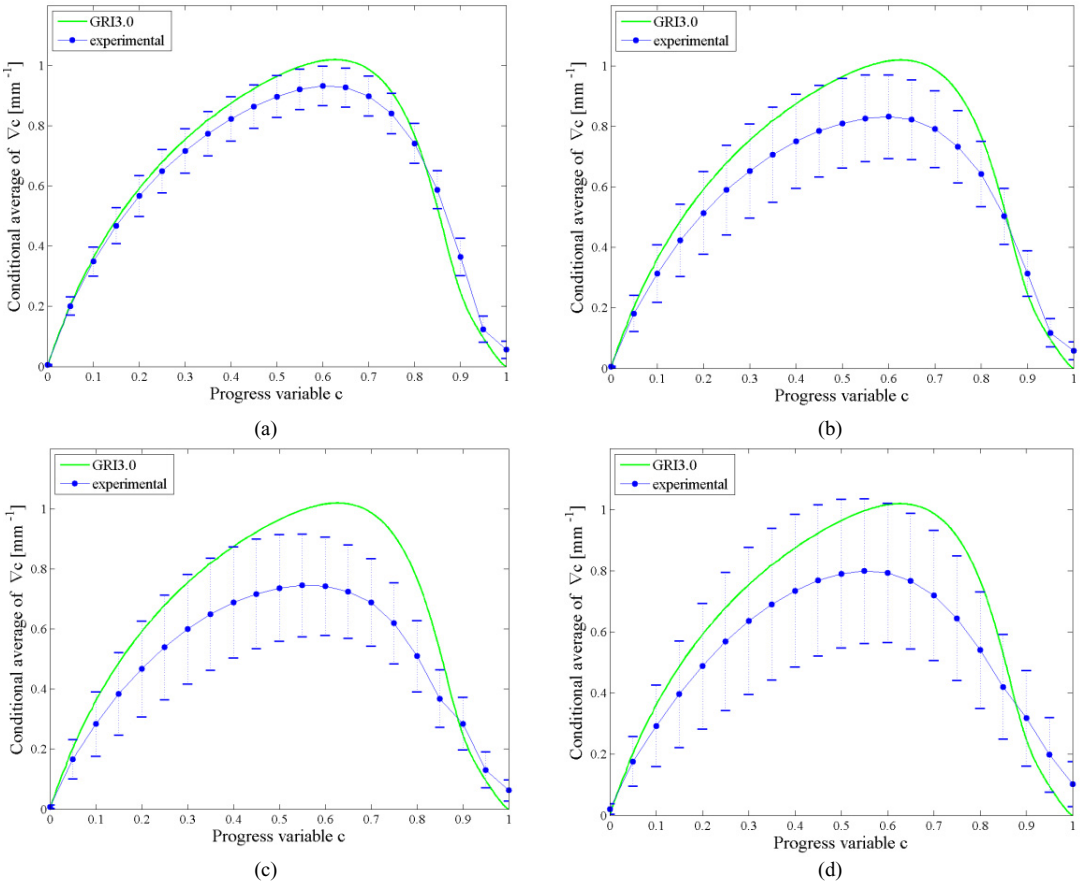

Fig.10 The progress variable gradient and its STD in turbulent contitions: (a) regime B (b) regime E (c) regime F (d) regime MH

Flame thickness is a good indicator of the quality of the Rayleigh scattering measurements and is directly related to the maximum of the temperature gradient by:

$$\delta = \left(T_b - T_u\right) / \nabla T_{\max} \tag{7}$$

The variation of flame thickness PDF with turbulence intensity is plotted in Fig. 11. The PDF is computed on the

iso-contour where the average of the progress variable is maximum. An iso-contour is determined by considering a linear interpolation between the values determined experimentally. For laminar regime a sharp peak is obtained due to a good experimental noise removal. The peak of the flame thickness PDF becomes smaller and the profile wider with increasing turbulence intensity. This is due to the fact that measurements are two dimensional and the third missing component becomes more and more important.

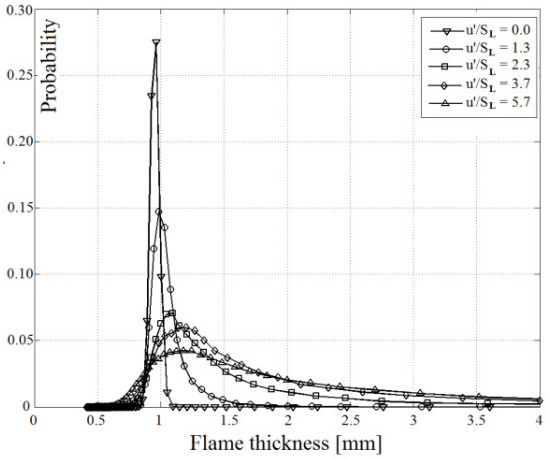

Fig.11. Influence of turbulence on flame thickness PDF

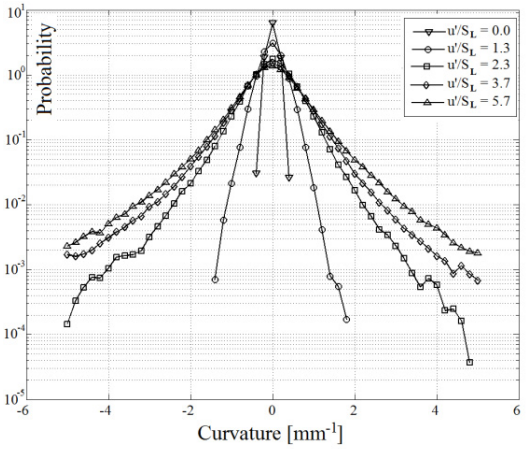

Fig.12 Influence of turbulence on curvature PDF

Flame curvature in each point along the flame front contours for c=0.5 can be obtained from the Rayleigh scattering images either in discrete or continuous two-dimensional forms. Discrete curvature is computed in a classical, geometrical mode, by calculating the radius of the circle passing through three near points of the given iso-contour c. The curvature is the reciprocal of the radius of the circle. To compute the iso-contour, a linear variation is assumed between two points (pixels) of the image. This linearization affects the accuracy of curvature but allows establishing correctly the sign by taking into account the position of the center of the circle. By convention, the curvature is positive if the center belongs to the burn side of the flame front. To increase the accuracy, the intensity of the local value of the scattering signal, I, can be used [22]:

$$K = \left[\frac{\partial I^2}{\partial x}\frac{\partial^2 I}{\partial y^2} - 2\frac{\partial I}{\partial x}\frac{\partial I}{\partial y}\frac{\partial^2 I}{\partial x \partial y} + \frac{\partial I^2}{\partial y}\frac{\partial^2 I}{\partial x^2} \right] \left(\frac{\partial I^2}{\partial x} + \frac{\partial I^2}{\partial y} \right)^{-3/2}. \quad (8)$$

The measured curvature statistics are 2-D quantities which may not be able to describe a 3-D phenomenon. However, Chen et. al [23] showed that 2-D and 3-D curvature PDFs are very similar and consequently the 2D measurements from a single laser sheet is good enough to capture the essential features of the curvature statistics. The influence of turbulent intensity over curvature probability is plotted in Fig. 12 which displays Gaussian-like distribution for all regimes. The PDF peaks are centred in zero and decrease as the turbulence intensity increase and more wrinkles disrupt the flame front. For low turbulent intensity the curvature PDF remain symmetric; however, the probability of negative curvature slightly increases with increasing turbulence.

A more detailed analysis can be done by computing the joint PDF of curvature and the maximum progress variable gradient which is related to flame thickness. For laminar combustion (Fig. 13-a), the joint PDF is symmetrical and there is no difference in gradient variation between positive and negative curvature.

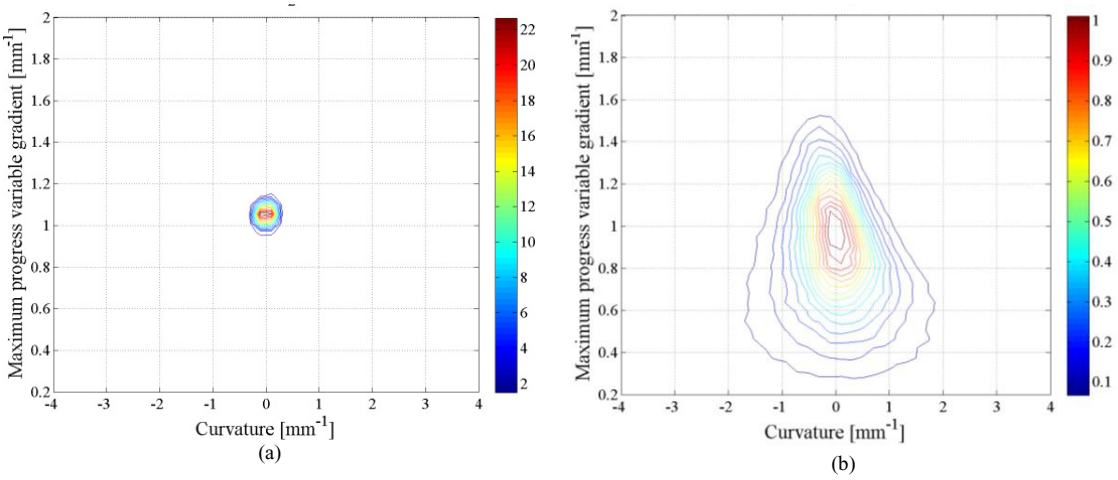

Fig.13. Joint PDF curvature/maximum progress variable gradient: (a) laminar flame (b) turbulent flame regime MH

As turbulence increases, the join PDF has a tendency to rotate counterclockwise and shift to the left side for negative curvature. The counterclockwise rotation indicates that negative curvature leads to increase of the progress variable gradient, while the positive curvature leads to diminish this gradient. The negative curvature brings more heat in the preheat zone and makes the temperature to increase faster, preheating reactants and so, the combustion is enhanced [24]. On the contrary, the positive curvature dissipates more heat and inhibits combustion.

5. Conclusions

Two-dimensional Rayleigh scattering technique is applied to a V-shaped flame of lean premixed methane-air mixture to investigate instantaneous temperature and the structure of flame front. Spatial resolution (expressed in terms of maximum temperature gradient) and the images post-processing have been validated with respect to numerical data for laminar flames. Then, thermal structures of turbulent flames are preliminary investigated for various turbulence intensities at quasi constant integral turbulent length scale on the combustion diagram. This analysis is performed first by computing the two-dimensional temperature gradient, which directly represents the flame surface density.

As it is known, the temperature gradients in turbulent flows are lower than in laminar case, mainly due to the two-dimensional characteristic of the optical technique. In fact the turbulent flows are intrinsic three-dimensional due the presence of random fluctuations. The results reflect an increased measurement uncertainty for high turbulence, where the standard deviation with respect to numerical data is greater.

Further investigations have been done to investigate the flame front structure. The flame front thickness PDF and the curvature PDF decrease with the turbulence intensity. The joint PDF of curvature and the maximum progress variable gradient have a tendency to rotate counterclockwise with the increase of turbulence intensity, negative curvature bringing more heat in the preheat zone which enhances combustion and so, increases the temperature gradients.

Acknowledgements

This publication is based on the results obtained in CORIA laboratories at University Rouen and INSA Rouen in France. This research was partially supported by the by the Joint Applied Research Project PN-II-PT-PCCA-2013-4, with the support of ANCS, CNDI – UEFISCDI, project no. 286/2014.

References

[1] Borghi R., Champion M., Modélisation et théorie des flammes *Technip*, Paris,2000.
[2] Pope S. B., The evolution of surfaces in turbulence. International Journal of Engineering Science , 26(5):445–469, 1988.
[3] Shepherd I. Flame surface density and burning rate in premixed turbulent flames. Proc Combust Inst, 26:373–9, 1996.
[4] Deschamps B.M., Smallwood G.J., Prieur J., Snelling D.R., Guulder O.L., Surface density measurements of turbulent premixed flames. Proc Combust Inst, 26:427–39, 1996.
[5] Lee G.G., Huh K.Y., Kobayashi H., Measurement and analysis of flame surface density for turbulent premixed combustion on a nozzle-type burner. Combust Flame, 122:43–57, 2000.
[6] Chen Y.C. and Bilger R.W.. Experimental investigation of three-dimensional flame-front structure in premixed turbulent combustion I: hydrocarbon/air Bunsen flames. Combustion and Flame, 131(4):400–435, 2002.
[7] Bell J.B., Day M.S., Grcar J.F., Lijewski M.J., Driscoll J.F., Filatyev S.A., Numerical simulation of a laboratory-scale turbulent slot flame. Proc Combust Inst 2006; 31:1299–307.
[8] Veynante D., Duclos J.M., Piana J., Experimental analysis of flamelet models for premixed turbulent combustion. Proc Combust Inst, 25:1249–56, 1994.
[9] Veynante D., Lodato G., Domingo P., Vervisch L.,. Hawkes E. R., Estimation of three-dimensional flame surface densities from planar images in turbulent premixed combustion, Exp. in Fluids, 49:267-278, 2010.
[10] Shepherd I.G., Cheng R.K., The burning rate of premixed flames in moderate and intense turbulence., Combust Flame, 127:2066–75., 2001
[11] Shepherd I.G., Cheng R.K., Plessing T., Kortschik C., Peters N., Premixed flame front structure in intense turbulence. Proc Combust Inst, 29:1833–40, 2002.
[12] Lawn C.J., Schefer R.W., Scaling of premixed turbulent flames in the corrugated regime. Combust Flame,146:180–99, 2006.
[13] Renou B., Mura A., Samson E., et al. Characterization of the local flame structure and the flame surface density for freely propagating premixed flames at various Lewis numbers. Combust Sci Technol, 174:143–79, 2002.
[14] Shy S.S., Lee E.I., Chang N.W., et al. Direct and indirect measurements of flame surface density, orientation, and curvature for premixed turbulent combustion modeling in a cruciform burner. Proc Combust Inst, 28:383–90, 2000.
[15] Sweeney M.S., Hochgreb S., Dunn M.J., and Barlow R.S. A comparative analysis of flame surface density metrics in premixed and stratified flames. Proceedings of the Combustion Institute , 32, 1419-1427, 2011.
[16] Clemens, N. T.,Flow Imaging,Encyclopedia of Imaging Science and Technology, Wiley, Hoboken, NJ, 2002, pp. 390–419
[17] Mazellier N., Danaila L., Renou B., Multi-scale energy injection: a new tool to generate intense homogeneous and isotropic turbulence for premixed combustion, *Journal of Turbulence*, **11**, N 43, 2010.
[18] Sneep M., Ubachs W., Direct measurement of the Rayleigh scattering cross section in various gases. *J. Quant. Spectrosc. Radiat.Transfer* **92** 293–310, 2005.
[19] Lafay Y., Renou B., Cabot G., Boukhalfa M., Experimental and numerical investigation of the effect of H2 enrichment on laminar methane–air flame thickness, *Combustion and Flame* **153** 540–561, 2008.
[20] Chen Y.C., Bilger R., Simultaneous 2-D imaging measurements of reaction progress variable and OH radical concentration in turbulent premixed flames: Experimental methods and flame brush structure. *Combust. Sci. and Tech* **167** 131-167, 2001.
[21] Chen Y.C., Bilger R.W., Experimental investigation of three-dimensional flame-front structure in premixed turbulent combustion I: hydrocarbon/air Bunsen flames. Combustion and Flame, **131**(4):400–435, 2002.
[22] Kass M., Witkin A., Terzopoulos D. Snakes: Active contour models. *International Journal of Computer Vision*, **1**(4):321–331, 1988.
[23] Chen Y. C., Kim M., Han J., Yun S., and Yoon Y., Analysis of flame surface normal and curvature measured in turbulent premixed stagnation-point flames with crossed-plane tomography. *Proc. Combust. Inst*. **31**:1327–1335, 2007
[24] Lafay Y., Renou B., Leventiu C., Cabot G., Boukhalfa A., Thermal Structure of Laminar Methane/Air Flames: Influence of H2 Enrichment and Reactants Preheating, *Comb. Sci. and Tech.*, **181**(9),1145-1163, 2009.